



# Effects of Er<sup>3+</sup> doping on the structure and electro-optical properties of 0.94(K<sub>0.5</sub>Na<sub>0.5</sub>)NbO<sub>3</sub>–0.06Sr(Zn<sub>1/3</sub>Nb<sub>2/3</sub>)O<sub>3</sub> ceramics

JIANGTING WANG<sup>1</sup>, YABING SUN<sup>1</sup>, SHAOYANG SHI<sup>1</sup>, HUA WANG<sup>1,2,\*</sup>, JIWEN XU<sup>1,2</sup>,  
LING YANG<sup>1,2</sup> and WEI QIU<sup>1,2</sup>

<sup>1</sup>School of Materials Science and Engineering, Guilin University of Electronic Technology, Guilin 541004, People's Republic of China

<sup>2</sup>Guangxi Key Laboratory of Information Materials, Guilin University of Electronic Technology, Guilin 541004, People's Republic of China

\*Author for correspondence (wh65@tom.com)

MS received 9 June 2021; accepted 16 September 2021

**Abstract.** The traditional solid-phase reaction method was used to dope the 0.94(k<sub>0.5</sub>Na<sub>0.5</sub>)NbO<sub>3</sub>–0.06Sr(Zn<sub>1/3</sub>Nb<sub>2/3</sub>)O<sub>3</sub> (0.94KNN–0.06SZN) with rare-earth Er<sup>3+</sup>, showing that the transparent ferroelectric ceramics have both up-conversion luminescence. Also the changes in the phase structure, optoelectronic properties of the ceramics after Er<sup>3+</sup> doping were investigated. The results show that the doping of Er<sup>3+</sup> has no significant effect on the phase structure, dielectric constant, coercivity field and residual polarization intensity of the ceramics. With the increase of Er<sup>3+</sup> content, the saturation polarization intensity shows a trend of decreasing and then increasing, and the dielectric constant first decreases and then stabilizes. The large amount of Er<sup>3+</sup> also greatly reduced the light transmission of the ceramics. In addition, the doping of Er<sup>3+</sup> gives the ceramics new properties. Under 980 nm laser excitation, the ceramics exhibit luminescent emission bands at 533, 554 nm (green) and 672 nm (red). The luminous intensity of the ceramic first strengthens with the increase of Er<sup>3+</sup> content and then weakens, and the strongest luminous intensity is obtained when the Er<sup>3+</sup> content is 1.00% mol. Transparent ferroelectric ceramics with light-emitting functions will have a broad application prospect in the field of photoelectric crossover.

**Keywords.** 0.94KNN–0.06SZN-*x*%Er; structure adjustment; photoelectric properties.

## 1. Introduction

Ferroelectric ceramics with outstanding properties, such as ferroelectricity [1], dielectricity [2], piezoelectricity [3], energy storage [4], electro-optical effects [5], have been widely used in the electronic functional device. Among ferroelectric ceramics, transparent ferroelectric ceramics have attracted research interest because of their excellent performance in optics and electrics [6–9].

Lead-containing ceramics have excellent electrical properties [6] and also have good light transmission [10]. Therefore, these materials are more intensively studied and used in practice among ferroelectric transparent ceramics. However, these materials contain lead and their use is restricted. There is an urgent need to investigate functional ceramics with ferroelectric, transparent and other properties to replace lead-containing ceramics. For example, in energy storage, Nd-doped barium titanate ceramics have the potential to replace lead-containing ceramics because they can be optimized for high energy density and efficiency through multi-component solid solution [11], and in

ferroelectricity and transparency, (K, Na)NbO<sub>3</sub> (KNN) system ceramics have great research and application prospects [12].

The ABO<sub>3</sub>-type structure of KNN has excellent ferroelectric and piezoelectric properties. The solid solution of KNN with a second component can further improve its electrical properties [13,14]. In the course of studying KNN ceramics, it was found that they also have some light transmission, subsequently, KNN-based lead-free transparent ferroelectric ceramics became a hot research topic [15–18]. Many conditions need to be met for a ceramic to be light transmissive, such as uniform grain size, absence of a second phase at the boundary and symmetrical crystal structure [19]. The pure KNN crystal structure has low symmetry, making it difficult to have high light transmission. The KNN-based transparent ferroelectric ceramics with symmetrical crystal structure can be made by adding a second component with a tetragonal structure [18,20–22].

In recent years, fluorescent materials have also become a hot spot for research, but it is difficult to fully utilize the internal luminescence of general fluorescent materials.

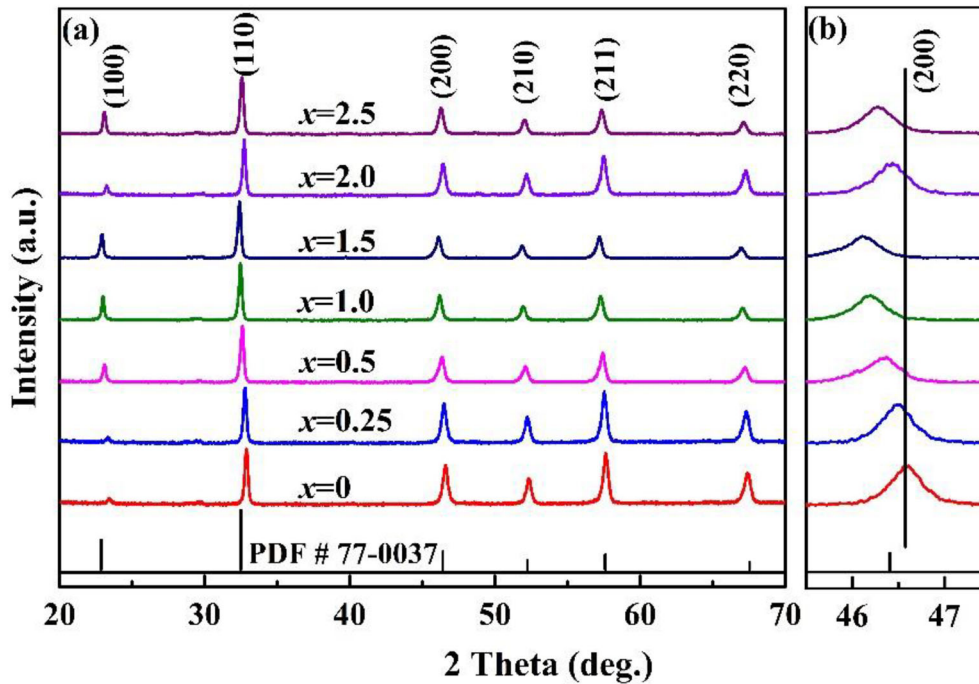


**Figure 1.** (a) XRD patterns of ceramic 0.94 KNN–0.06SZN– $x\%$ Er. (b) Enlarged XRD patterns in the  $2\theta$  range of 46–47°.

**Table 1.** Lattice parameters of 0.94KNN–0.06SZN– $x\%$ Er ceramics.

$x$	$a$ (Å)	$b$ (Å)	$c$ (Å)	$V$ (Å <sup>3</sup> )	$c/a$
0	5.562	5.544	3.958	122.042	0.717
0.25	5.580	5.578	3.960	123.265	0.710
0.50	5.592	5.597	3.965	124.089	0.709
1.00	5.616	5.635	3.973	125.708	0.707
1.50	5.680	5.669	3.997	128.699	0.704
2.00	5.643	5.648	3.957	126.123	0.701
2.50	5.592	5.610	3.898	122.262	0.697

Fluorescent materials based on transparent ceramics can compensate for this deficiency and effectively increase luminescence utilization. Doping rare earth in KNN-based transparent ferroelectric ceramics can make them more functional and have more promising applications [23–27]. Er<sup>3+</sup> has a unique 4f electron layer, which is shielded by the 5s and 5p electron shell layers so that the electrons in the 4f energy level emit at wavelengths unaffected by the subject material when they leap [28]. Zhao *et al* [24] found that Er<sup>3+</sup> significantly improved the photoluminescence performance of the [Li<sub>0.04</sub>(K<sub>0.49</sub>Na<sub>0.51</sub>)<sub>0.96</sub>]NbO<sub>3</sub>– $x$ Er<sub>2</sub>O<sub>3</sub> ceramics. The (K<sub>0.5</sub>Na<sub>0.5</sub>)<sub>0.95</sub>Li<sub>0.05</sub>Nb<sub>0.95</sub>Bi<sub>0.05</sub>O<sub>3</sub>–1%Er<sub>2</sub>O<sub>3</sub> ceramic has up-conversion luminescence and photochromic response properties, which was prepared using the pressureless sintering method by Sun *et al* [25]. These experimental

results show that Er has high luminescence efficiency and Er-doped KNN-based ceramics have up-conversion luminescence properties. Therefore, Er is one of the preferred rare-earth elements in the study of KNN-based fluorescent ceramics.

Chai *et al* [12] had synthesized K<sub>0.5</sub>Na<sub>0.5</sub>NbO<sub>3</sub>– $x$ Sr(Zn<sub>1/3</sub>Nb<sub>2/3</sub>)O<sub>3</sub> with high light transmittance, excellent ferroelectricity and other outstanding properties, using the traditional solid-phase reaction method. The study showed that the best performance of the ceramic in all aspects was achieved at  $x = 0.06$ . Such multifunctional ceramics will be of greater research significance if they also have light-emitting properties. This work is based on the study of Chai *et al* [12], in which the Er<sup>3+</sup>-doped 0.94(K<sub>0.5</sub>Na<sub>0.5</sub>)NbO<sub>3</sub>–0.06Sr(Zn<sub>1/3</sub>Nb<sub>2/3</sub>)O<sub>3</sub> ceramics with photoluminescence properties were prepared by the conventional solid-phase method, and the principle of luminescence was elaborated. The effects of Er<sup>3+</sup> on the microstructure, optical and electrical properties were investigated.

## 2. Experiment

### 2.1 Material preparation

0.94(k<sub>0.5</sub>Na<sub>0.5</sub>)NbO<sub>3</sub>–0.06Sr(Zn<sub>1/3</sub>Nb<sub>2/3</sub>)O<sub>3</sub>– $x\%$ Er (0.94KNN–0.06SZN– $x\%$ Er) ceramics were fabricated by conventional solid-phase approach. Na<sub>2</sub>CO<sub>3</sub> (≥99.5%), K<sub>2</sub>CO<sub>3</sub> (≥99%), Nb<sub>2</sub>O<sub>5</sub> (≥99.99%), SrCO<sub>3</sub> (≥99.99%), ZnO (≥99.9%) and Er<sub>2</sub>O<sub>3</sub> (≥99.5%) were used in this

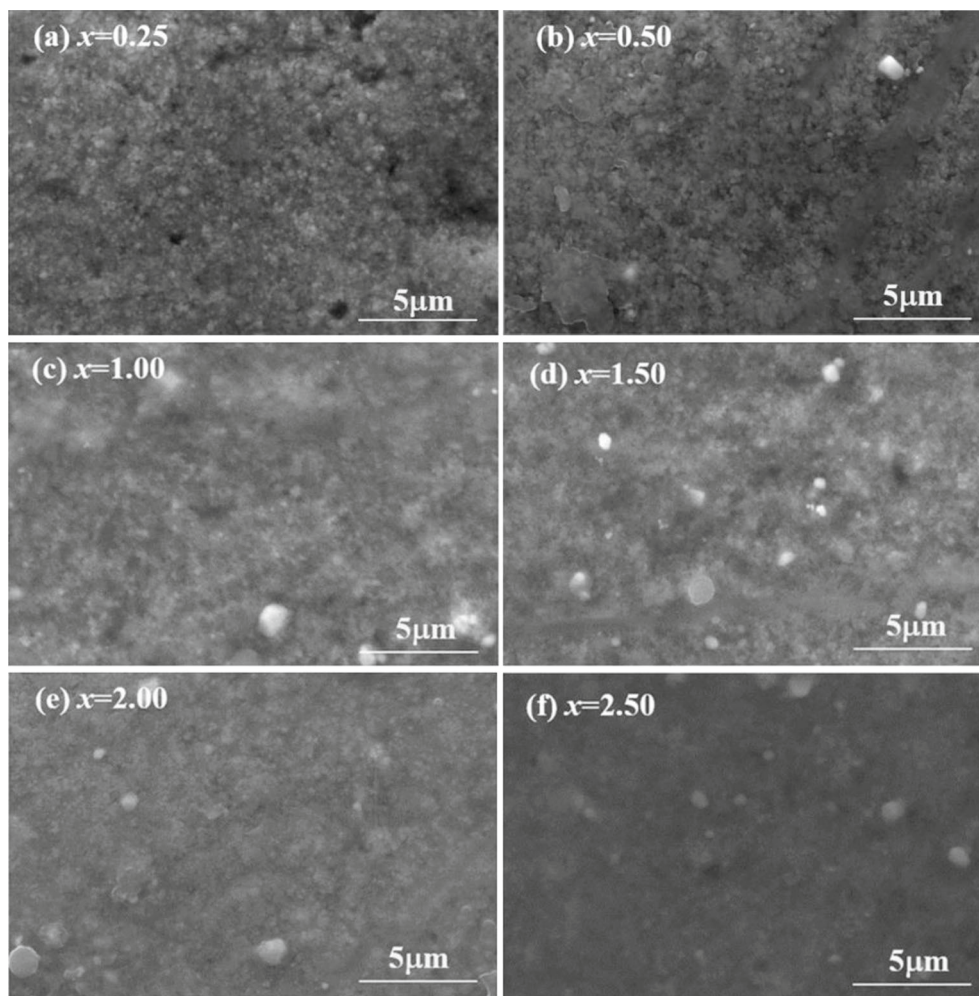


**Figure 2.** SEM images of 0.94KNN–0.06SZN– $x\%$ Er ceramics.

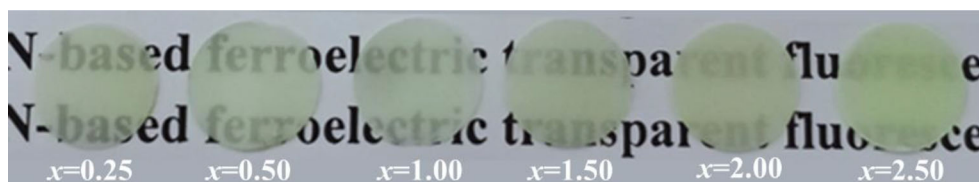


**Figure 3.** Picture of 0.94KNN–0.06SZN– $x\%$ Er ceramics.

experiment. These raw materials were dried in a drying oven at 70°C for more than 24 h before being weighed. These powders and ZrO<sub>2</sub> balls were mixed with anhydrous ethanol and ball-milled for 24 h. The dried powders were put into the muffle furnace and calcined at 900°C for 3 h. The calcined powder was ball-milled again under the same conditions. The 7 wt% polyvinyl alcohol was uniformly mixed with the powder and then passed a 100-mesh sieve. These powders were pressed into circular tablets of 1 mm thickness and 12 mm diameter. The green bodies were sintered at 1180–1200°C for 3 h in double sealed alumina crucibles. Finally, the obtained specimens were polished to 0.3 mm thickness.

## 2.2 Characterization

The crystal structure was determined by X-ray diffractometer (XRD, PANalytical Empyrean 2, Panalytical, The Netherlands). The microstructure was obtained by a field-emission scanning electron microscopy (Quanta FEG-450, FEI Company, USA). Temperature-dependent dielectric properties were measured by impedance analyzer (Agilent 4294A, USA). Hysteresis loops ( $P$ – $E$ ) were tested using a ferroelectric system (TF Analyzer 2000HS, Germany). Measurement of fluorescence spectra was done by spectrophotometer (SENS-9000A, Zolix).

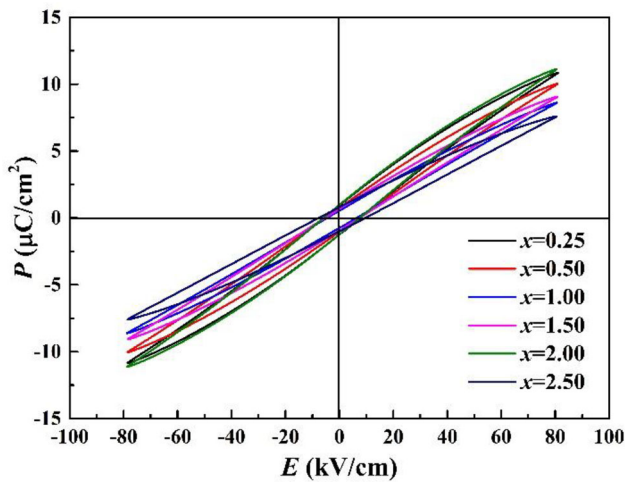


**Figure 4.** Room temperature  $P$ - $E$  hysteresis loops of 0.94KNN-0.06SZN- $x\%$ Er ceramics.

### 3. Results and analysis

Figure 1a shows the XRD patterns of the ceramic samples in  $2\theta$  in the range of  $20^\circ$  to  $70^\circ$ . All samples have a typical perovskite structure and the characteristic peaks match the PDF card (PDF # 27-0788) of  $\text{Na}_{0.5}\text{Sr}_{0.25}\text{NbO}_3$ . This indicates that the  $\text{Er}^{3+}$  has completely entered the 0.94KNN-0.06SZN lattice, forming a single stable phase structure [29]. To further analyse the influence of  $\text{Er}^{3+}$  on the ceramic phase structure, the (200) diffraction peak was amplified, as shown in figure 1b. The (200) diffraction peaks of all ceramics are single and no separate peaks are generated. This phenomenon shows that the ceramics are still pseudocubic structures [22]. Based on the Bragg equation, the diffraction peaks shift is due to a change in the crystal plane spacing. There are differences between the ionic radius and chemical valence of  $\text{Er}^{3+}$  and other ions in ceramics. The substitution of  $\text{Er}^{3+}$  for other ions leads to a change in the crystal plane spacing, which causes a shift in the diffraction peaks [30]. The lattice constants of ceramics are shown in table 1, indicating the lattice distortion of ceramics. The ionic radius of  $\text{Er}^{3+}$  is 0.089 nm and the coordination number is 6 (CN=6), which will preferentially replace ions with a similar ionic radius during the doping process. The radii of each ion in the ceramic lattice are  $\text{Na}^+$  (0.102 nm, CN=12),  $\text{K}^+$  (0.138 nm, CN=12) and  $\text{Sr}^{2+}$  (0.118 nm, CN=12) in the A-sites, as well as that  $\text{Zn}^{2+}$  (0.074 nm, CN=6) and  $\text{Nb}^{5+}$  (0.064 nm, CN=6) in the B-sites. In comparison,  $\text{Er}^{3+}$  will have replaces of  $\text{Zn}^{2+}$  first and then  $\text{Nb}^{5+}$ .  $\text{Er}^{3+}$  has a bigger ionic radius and higher chemical valence than  $\text{Zn}^{2+}$  under similar coordination number, so it causes lattice expansion when replacing  $\text{Zn}^{2+}$ , resulting in a larger crystal plane spacing in ceramics. Therefore, the diffraction peaks of XRD are shifted to a lower angle [31]. Because the chemical valence of  $\text{Nb}^{5+}$  is higher than that of  $\text{Er}^{3+}$ , the ceramic lattice collapses during the substitution of

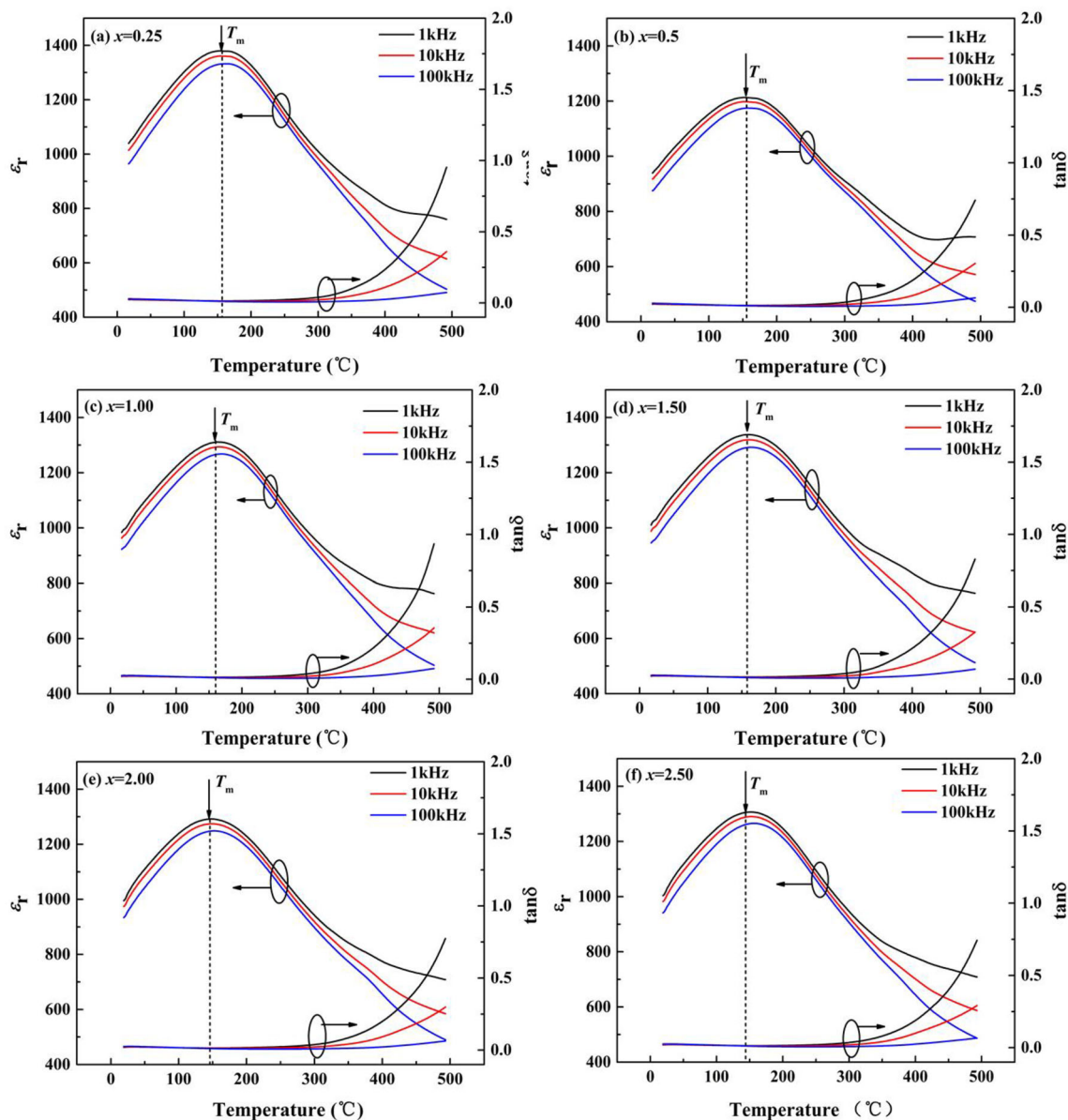
$\text{Nb}^{5+}$  by  $\text{Er}^{3+}$ . The lattice contraction of the ceramic causes the diffraction peaks to start shifting to a higher angle [32].

Figure 2 shows the surface morphology of the 0.94KNN-0.06SZN- $x\%$ Er ceramics. When  $x = 0.25$ , the grains on the surface of the ceramic are very fine. With the increase of the rare-earth  $\text{Er}^{3+}$  doping content, abnormally grown grains start to appear on the ceramic surface from  $x = 1.00$ . This result indicates that rare-earth  $\text{Er}^{3+}$  can promote the growth of ceramic grains and make them larger. But overall, the grain size is still fine and uniform. The presence of abnormally large grains is one of the reasons for the reduced transparency of ceramics [17]. Figure 3 shows the picture of the ceramics (0.3 mm thickness). The lettering under the ceramics gradually blurs as the  $\text{Er}^{3+}$  content increases, which also indicates that the addition of rare earth significantly reduces the transparency of the ceramics.

Figure 4 shows the room temperature hysteresis loops ( $P$ - $E$  loops) of 0.94KNN-0.06SZN- $x\%$ Er ceramics at  $f = 1$  Hz and  $E_b = 80$  kV  $\text{cm}^{-1}$ . The  $P$ - $E$  curve shows a slender shape. It can be preliminary judged that the 0.94KNN-0.06SZN- $x\%$ Er $^{3+}$  are relaxed ferroelectrics.  $\text{Er}^{3+}$  has no significant effect on the remanent polarization ( $P_r$ ) and coercive field ( $E_c$ ) of the ceramic. The maximum polarization intensity ( $P_{\text{max}}$ ) decreases first and then increases with the increase of  $\text{Er}^{3+}$  content. When  $x = 2.00$ , a large amount of  $\text{Er}^{3+}$  caused the ceramic lattice to shrink and increase the oxygen vacancies, leading the ceramic easier to be polarized. The excessive oxygen vacancies also weaken the actual field strength inside the ceramic, resulting in  $P_{\text{max}}$  sudden drop when  $x = 2.50$ . This phenomenon corresponds to the variation in the lattice size of the ceramics shown in the XRD analysis.

Figure 5 shows the dielectric temperature spectrum of ceramics at different frequencies. Relaxed ferroelectrics have no specific Curie temperature. The temperature ( $T_m$ ), corresponding to the maximum dielectric constants, is generally used as the characteristic temperature. The doping of  $\text{Er}^{3+}$  does not have much effect on the  $T_m$  of ceramics. As the  $\text{Er}^{3+}$  content increases, the  $T_m$  move to lower temperatures, but the magnitude of the movement is not significant. It can be seen from the figure that the  $T_m$  value of all specimens is around  $150^\circ\text{C}$  ( $0.25 \leq x \leq 0.50$ ). The  $T_m$  decreases to below  $100^\circ\text{C}$  from  $x \geq 2.00$ . The maximum dielectric constant of ceramics first decreases and then tends to be stable. When the value of  $x$  increases from 0.25 to 0.50, the dielectric constant decreases from 1380 to 1200. Since then,  $1.00 \leq x \leq 2.50$ , the dielectric constant remains around 1300. The replacement of  $\text{Zn}^{2+}$  by  $\text{Er}^{3+}$  causes the ceramic lattice to swell, expanding the range of  $\text{NbO}_6$  activity and making the ceramic more susceptible to polarization [33]. In addition, in the process of replacing  $\text{Nb}^{5+}$  by  $\text{Er}^{3+}$ , oxygen vacancies are created to maintain charge balance, which disrupts the  $\text{NbO}_6$  octahedral structure and lead to the collapse of the ceramic lattice, so the dielectric response of the ceramic becomes weaker and the dielectric constant decreases [34].





**Figure 5.** Temperature dependence of dielectric constant ( $\epsilon_r$ ) and dielectric loss ( $\tan \delta$ ) of 0.94KNN–0.06SZN– $x\%$ Er ceramics.

From the dielectric temperature spectrum, frequency dispersion occurs below the Curie Peak. The degree of frequency dispersion is measured by the dispersion index ( $\gamma$ ), which is usually used to determine the properties of ferroelectrics.  $\gamma = 1$  and 2 correspond to normal ferroelectrics and ideal relaxed ferroelectrics, respectively. The  $\gamma$  can be fitted from the relationship curves of  $\ln(1/\epsilon - 1/\epsilon_m)$  and  $\ln(T - T_m)$  curves [2], as shown in figure 6. The  $\gamma$  of all ceramics ( $0.25 \leq x \leq 2.50$ ) is between 1.75 and 1.87, and relatively closer to 2. So, it can be finally judged that the ceramics 0.94KNN–0.06SZN– $x\%$ Er are relaxor ferroelectric.

Figure 7 shows the up-conversion emission spectrum under the excitation of 980 nm light. The ceramic

0.94KNN–0.06SZN–0.25%Er appears as a green luminescent band with a luminescent centre at 550 nm and a red emission band with a luminescent centre at 664 nm with weak intensity. The other component points ( $x = 0.50, 1.00, 1.50, 2.00, 2.50$ ) show two green emission peaks at 533 and 554 nm, and a red emission peak with higher intensity at 672 nm. The reason for these emission peaks is the jump between the energy levels of electrons, corresponding to  $^2H_{11/2} \rightarrow ^4I_{15/2}$  (533 nm),  $^4S_{3/2} \rightarrow ^4I_{15/2}$  (554 nm) and  $^4F_{9/2} \rightarrow ^4I_{15/2}$  (672 nm), respectively [35]. As can be seen from the figure, the photoluminescence intensity of the ceramics gradually increases at first ( $0.25 \leq x \leq 1.00$ ), reaches its maximum intensity at 1.00, and then decreases ( $1.00 \leq x \leq 2.50$ ).

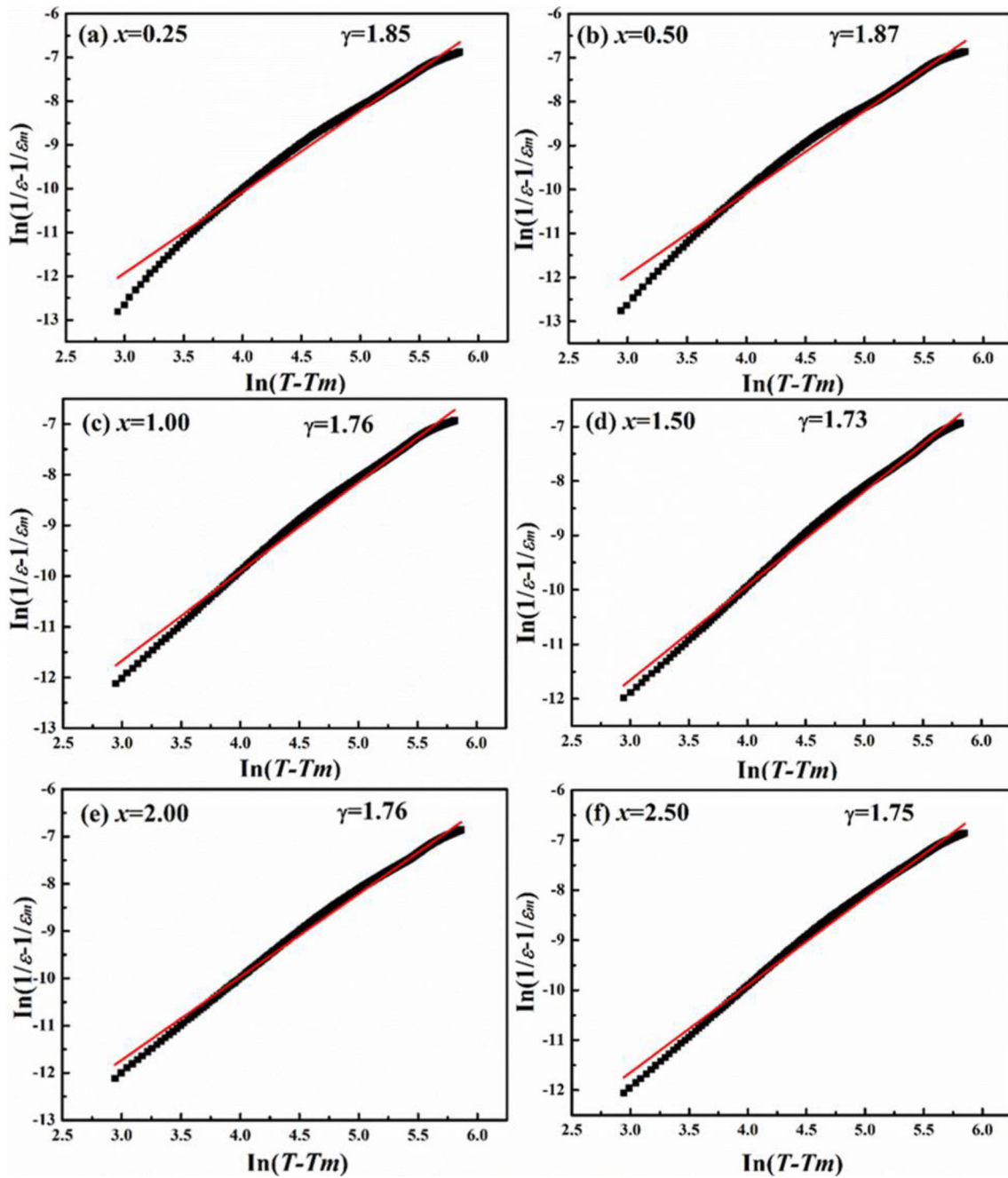


**Figure 6.** Dispersion index of 0.94KNN–0.06SZN– $x\%$ Er ceramics.

Figure 8 is the schematic diagram of the up-conversion luminescence principle of  $\text{Er}^{3+}$  in ceramics. Under the excitation of 980 nm optical laser, the  $\text{Er}^{3+}$  absorbs energy and jump from the ground state to energy level  $^4I_{11/2}$  first, after which some  $\text{Er}^{3+}$  filled the  $^4F_{7/2}$  energy levels through a continuous multiphoton absorption process. Then phonon relaxation occurs to make the  $\text{Er}^{3+}$  fill the lower energy levels  $^2H_{11/2} \rightarrow ^4I_{15/2}$ ,  $^4S_{3/2} \rightarrow ^4I_{15/2}$  and  $^4F_{9/2} \rightarrow ^4I_{15/2}$ . Therefore, two green light emission peaks and one red light

emission peak are generated [36]. The luminescence intensity of rare-earth ions is related to the symmetry of the substrate structure [37]. At  $x = 0.25$ , the luminescence intensity is weakest, due to the small amount of  $\text{Er}^{3+}$  that has not yet changed the symmetrical cubic structure of the ceramics. At  $x \geq 1.00$ , too much  $\text{Er}^{3+}$  undergoes cross-relaxation, resulting in a concentration-dependent burst of photoluminescence. The luminescence of ceramics was weakened after continuing to increase the  $\text{Er}^{3+}$  content.

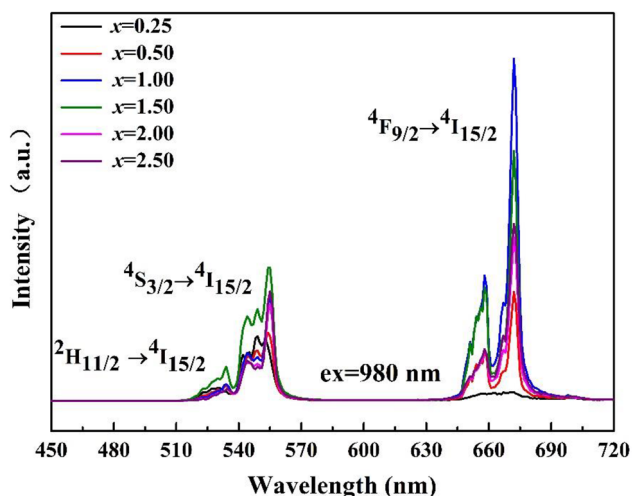


Figure 7. Up-conversion luminescence patterns of 0.94KNN-0.06SZN- $x\%$ Er ceramics.

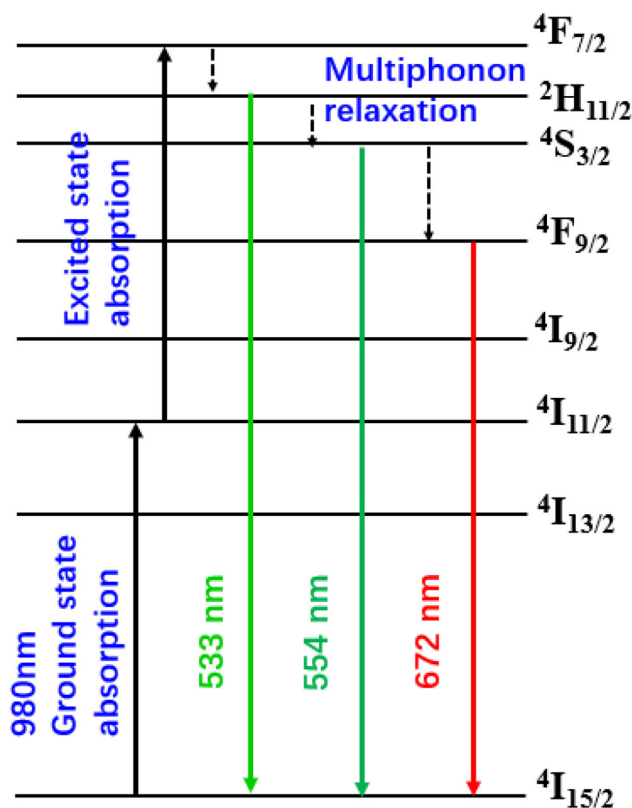


Figure 8. Schematic diagram of the up-conversion luminescence principle of  $\text{Er}^{3+}$  in ceramics.

#### 4. Conclusions

0.94KNN-0.06SZN- $x\%$ Er ceramics were prepared by the conventional solid-phase method. The  $\text{Er}^{3+}$  allowed the ceramic to acquire photoluminescence properties. Two emission peaks of green light (554 and 533 nm) and one red light (672 nm) appear, and the 0.94KNN-0.06SZN-1.00%Er having the highest luminescence intensity. The

$\text{Er}^{3+}$ -doped ceramics is pseudo-cubic in structure, but the optical permeability of ceramics declined. The  $\text{Er}^{3+}$ -doped ceramics are relaxed ferroelectrics. The dielectric constant reaches a minimum at  $x = 0.5$  and then stabilizes at about 1350. Rare-earth-doped KNN-based ferroelectric transparent fluorescent ceramics retain excellent electrical properties at the same time. Multifunctional ceramics with optical and electrical properties have more research significance and application prospects.

#### Acknowledgements

This study was supported by the National Nature Science Foundation of China (61965007) and Guangxi Nature Science Foundation (2018GXNSFDA281042).

#### References

- [1] Nanakorn N, Jalupoom P, Vaneesorn N and Thanaboonsombut A 2008 *Ceram. Int.* **34** 779
- [2] Fuentes J, Portelles J, Durruthy-Rodríguez M D, H'Mok H, Raymond O, Heiras J *et al* 2015 *Appl. Phys. A* **118** 709
- [3] Wang H, Zhai X, Xu J W and Yang L 2016 *J. Mater. Sci.: Mater. Electron.* **27** 8217
- [4] Yang H B, Yan F, Lin Y, Wang T, Wang F, Wang Y L *et al* 2017 *J. Eur. Ceram. Soc.* **37** 3303
- [5] Kamzina L S, Ruan W, Li G R and Zeng J T 2012 *Phys. Solid State* **54** 2024
- [6] Ma Z M, Zhang Y C, Lu C J, Qin Y L, Lv Z L and Lu S J 2018 *J. Mater. Sci.: Mater. Electron.* **29** 6985
- [7] Li F L and Kwok K W 2013 *J. Eur. Ceram. Soc.* **33** 123
- [8] Qiu C R, Wang B, Zhang N, Zhang S J, Liu J F, Walker D *et al* 2020 *Nature* **577** 350
- [9] Ren X D, Jin L, Peng Z H, Chen B, Qiao X S, Wu D *et al* 2020 *Chem. Eng. J.* **390** 124566
- [10] Yin Q R, Ding A L, Zheng X S, Qiu P S, Shen M R and Cao W W 2004 *J. Mater. Res.* **19** 729
- [11] Sun Y B, Wang H, Liu G B, Xie H, Zhou C G, Chen G H *et al* 2020 *J. Mater. Sci.: Mater. Electron.* **31** 5546
- [12] Chai Q Z, Yang D, Zhao X M, Chao X L and Yang Z P 2018 *J. Am. Ceram. Soc.* **101** 2321
- [13] Wang H, Zhao X Y, Xu J W, Zhai X and Yang L 2016 *Bull. Mater. Sci.* **39** 743
- [14] Gio P D, Bau T T, Hoai N V and Nam N Q 2020 *J. Mater. Sci. Chem. Eng.* **8** 1
- [15] Du H L, Zhou W C, Zhu D M and Fa L 2008 *J. Am. Ceram. Soc.* **91** 2903
- [16] Qu B Y, Du H L and Yang Z T 2016 *J. Mater. Chem. C* **4** 1795
- [17] Zhao X M, Chai Q Z, Chen B, Chao X L and Yang Z P 2018 *J. Am. Ceram. Soc.* **101** 5127
- [18] Hu G B, Liu H N, Wang J T, Sun Y B, Wang H, Xu J W *et al* 2021 *J. Electron. Mater.* **50** 968
- [19] Zhang M, Yang H B, Li D and Lin Y 2020 *J. Alloys Compd.* **829** 154565
- [20] Zhang X S, Yang D, Yang Z Y, Zhao X M, Chai Q Z, Chao X L *et al* 2016 *Ceram. Int.* **42** 17963

- [21] Chai Q Z, Zhao X M, Chao X L and Yang Z P 2017 *R Soc. Chem.* **7** 28428
- [22] Xie H, Liu G B, Yang L, Pang S J, Yuan C L, Zhang X W *et al* 2018 *J. Mater. Sci.: Mater. Electron.* **29** 19123
- [23] Goldstein A and Krell A 2016 *J. Am. Ceram. Soc.* **99** 3173
- [24] Zhao Y J, Ge Y Y, Zhang X W, Zhao Y Z, Zhou H P, Li J B *et al* 2016 *J. Alloys Compd.* **683** 171
- [25] Sun H Q, Lv Y, Zhu Y, Lin J F, Wu X, Zhang Q W *et al* 2019 *J. Am. Ceram. Soc.* **102** 6732
- [26] Geng Z M, Li K, Li X and Shi D L 2017 *J. Mater. Sci.* **52** 2285
- [27] Wu X, Lin J F, Chen P F, Liu C W, Lin M, Lin C *et al* 2019 *J. Am. Ceram. Soc.* **102** 1249
- [28] Wu X, Kwok K W and Li F L 2013 *J. Alloys Compd.* **580** 88
- [29] Sun Y B, Wang H, Zhou C R, Yang L and Xu J W 2021 *Bull. Mater. Sci.* **44** 139
- [30] Zhao Y, Wang X S, Zhang Y, Li Y X and Yao X 2020 *ACS Appl. Electron. Mater.* **2** 3028
- [31] Zhou J, Ma Q, Wang P F, Cheng L J and Liu S J 2014 *Ceram. Int.* **40** 2451
- [32] Zhao X M, Chao X L, Wu D, Liang P F and Yang Z P 2019 *J. Alloys Compd.* **798** 669
- [33] Zhai Y Z, Feng Y, Du J, Xue J, Shen J, Lu Y *et al* 2019 *J. Mater. Sci.: Mater. Electron.* **30** 4352
- [34] Maziaty Akmal M H, Warikh A R M, Azlan U A A, Azam M A and Ismail S 2016 *Mater. Lett.* **170** 10
- [35] Liu J, Zhang Y, Sun H Q, Zhang Q W, Wang X S and Hao X H 2019 *J. Lumin.* **207** 85
- [36] Lin J F, Lu Q L, Wu X, Sun H L, Lin C, Lin T F *et al* 2019 *J. Mater. Chem. C* **7** 7885
- [37] Wu X, Lu S B and Kwok K W 2017 *J. Alloys Compd.* **695** 3573